

Filled shell approximation: two-way self-consistent linear response cross-over searching for DFT+U on full-filled d/f shell binary AB_x compounds (A=Zn, Cu, Cd, Ga, and Lu; B=O, S, N, P, and As; x > 0)

Bolong Huang

Department of Physics and Materials Science, City University of Hong Kong, Kowloon, Hong Kong SAR, China

Abstract

We proposed a two-way cross-over searching the U parameters for fulfilled shell compounds, which was inspired by the fluctuation of the electronic charge and magnetic moment in the constraint volume. This gives us another way of understanding the entanglement of strong *p-d* orbitals coupling for unraveling the screened Coulomb potential for ful-filled shells. This can also help us to have a quick look on the electronic structures of some potential low-dimensional or superconducting materials.

1. Introduction

Full/nearly-filled shell metal oxides like Copper (I) oxide (Cu_2O) and ZnO are semiconducting oxides can be used for filling the demands of current highly portable electronics. The Cu_2O is the prototype material of “invisible electronics” devices. ZnO can be used in low-dimensional nano-generator for generating electricity for portable electronics. Using DFT+U method on these materials, we can get quick answer of the electronic structures of the low dimensional atomic models. One can simply use linear response method to obtain the localized partially filled but it seems difficult to have correct estimation on the U for $3d^{10}$ configuration. The electron wavefunctions of $3d^{10}$ are indeed constrained with strict boundary conditions. Therefore the perturbation turns extremely small if we use a small Lagrange multiplier for perturbing the full-filled localized orbital. The consequence is the inverse of this small difference has the tendency of being a singularity (e.g. $1/\chi$ with $\chi \rightarrow 0$). Thus, the simple estimation of U parameter through the inverse of the small perturbation by linear response turns to be unphysical.

As is well known, the DFT+U formalism can be written as the first-order approximation to the GW method[1] in static limit, for solving the calculations with localized states, proved by Anisimov et al in the form of rotational invariant type DFT+U formalism[2]. Literature reported the self-interaction correction (SIC) can give improved electronic structure for d-orbital based materials like transition metal compounds though, it usually have large error of the d-orbital levels, which is about 1Ry below valence band[3]. On the other hand, DFT+U with U on localized d/f orbital is hardly give correct band gap for ZnO , even for $U_d=10$ eV. Therefore, we reformulate the process of solving the U parameter by linear response from Cococcioni et al.[4], and explore out the intrinsic properties of self-consistent Hubbard U determination calculation, it is indeed a static limit of cRPA and frequency independent[5, 6]. The advantage of our method is we do not need to solve complicated Green function based quasi-particle onsite screened Coulomb interaction W as GW does, at the same time, we over pass the difficulties of solving Hartree-Fock equations in hybrid functionals with semi-empirical determined Thomas-Fermi screening length[7]. Another positive propelling force for us is no need to calculate the zero point of linear responded value of Hubbard U since this can be easily and largely overestimated

for full-filled shells, we only focus on the difference value of the two types of self-consistent calculations of determining the U , and the systematic error of the conventional methodologies have been counteracted.

The description on localized hole state levels by DFT is another key issue for d/f orbital based metal oxides or similar compounds. For a metal vacancy site, the induced holes (removal of electrons) are usually localized and at the p- π orbitals of nearby O-sites, which denotes the levels near the valence band maximum (VBM). To accurately calculate these hole induced levels, it is necessary to consider the Hubbard U parameter for correcting the O-2p orbital energies in the metal oxides. These have been proved to largely improve the both electronic and defect formation energies as well as their single-particle levels in the band gap[8]. Indeed, there have been many theoretical topics urges us to use DFT+ U to balance the role played by holes. Like the non-equilibrium layer-by-layer epitaxially growth of oxides (LaAlO₃/SrTiO₃ interface), to investigate the Mott insulating states of the layered oxide interfaces, Pentcheva et al have applied U for O-2p orbital to correct the behavior of the localized $S=1/2$ hole residing on 2p valence band (with p- π feature)[9]. Even earlier study on layered superconductor materials, LaCuO₄ by McMahan et al, they use the same method for O-2p orbital to verify the Impurity Anderson Model for Cu-O based superconducting oxides[10]. These outcomes enhanced the reliability for finding the negative-effective-correlation energy (negative- U_{eff}) in Ga vacancy (V_{Ga}) in GaN for explaining the effects induced by magnetic elements doping[11].

To give a self-consistent determined Hubbard U parameter for filled shell compounds, the work of Agapito et al has recently improved the linear response technique by calculating out the electron repulsion energy with Hartree-Fock (HF)[12]. This gives reasonable U for both Zn-3d (12.8 eV) and O-2p (5.29 eV) in ZnO, but too small for Ti-3d (0.15 eV) in TiO₂ may largely underestimate the oxygen vacancy level next to the conduction band. Meanwhile, whether the correlation should be considered within the model of Agapito et al is still unknown, since the HF was only considered in calculating the electron-electron interactions. Meanwhile, as Clark et al pointed[7], the defect states should be also accurately described based on reasonable electronic structures. Thus, the reliability of self-consistent determined U for whatever the full-filled shell compounds is also an issue. Therefore, we need to propose a manner for PBE to natively describe the U in self-consistent way.

2. Methodology

Dederichs et al proposed a generalized model for processing the similar constraint linear response model by splitting the fluctuation of orbital occupancies into charge and magnetic moment fluctuations in certain volume V in the solid[13]. Our model is inspired by Dederichs et al that divide the perturbation of orbital occupancy in two ways.

Strictly speaking, in perturbation theory, to process the calculations of self-energy of an electron, should be considered into two directions. One, consider the original of the electrical potential $U(\mathbf{r})$ of the electron location constant, the local effect of the deviations of the electronic charge distribution from the range of \mathbf{r} to $\mathbf{r}+\epsilon$; Secondly, keep the original electronic charge distribution $q(\mathbf{r})$ constant, the local effect of the fluctuation of the electrical potential at the range of the \mathbf{r} to $\mathbf{r}+\epsilon$, and both the ϵ are very small, $\epsilon \ll 1$. Consider both the perturbation, we summarize into two different classes of the perturbations, one is the charge (electron orbital

occupancy) perturbation, another is the electronic potential perturbation. This treatment is actually is l -degenerated, l is the max angular momentum of the targeted electron orbital. When this two perturbation reach the equivalent effect, the input on-site Coulomb potential U_{eff} is the equivalent self-energy of the electron located at its orbital. This equivalent Coulomb potential is the right contribution of the electron Coulombic self-energy that generally considered the electron and electron itself. Regardless whether to be phenomenological to the description on Coulomb equivalent potential, at least we only consider the general perturbation from the aspect of the energy.

Then based on this concept, there always exists an input value of Hubbard-U in terms of:

$$h(U_{in}) = [g(U_{in}) - f(U_{in})] \quad (1)$$

The Eq (1) converges to zero or local minimum in physical meaning described above. If $g(U_{in})$ is charge occupancy perturbation and electronic potential perturbation for $f(U_{in})$, respectively. We refer the equations from the equations proposed by Kulik et al[14].

$$E_{\text{quad}} = \frac{U_{\text{scf}}}{2} \sum_I \left[\sum_i \lambda_i^I \left(\sum_j \lambda_j^I - 1 \right) \right] + \frac{U_{in}}{2} \sum_I \sum_i \lambda_i^I (1 - \lambda_i^I) \quad (2)$$

In Eq (2), the electronic terms of total energy in GGA+U functional have quadratic dependence on the occupations. The first term of Eq (2) represents the contribution of the double counting term of GGA+U functional, the second term is our general Anisimov-type customary DFT+U correction[2]. The U_{scf} from the Eq(2) represents the effective on-site electron-electron interaction of GGA functional for GGA+U ground state when U is chosen to be U_{in} . A strong consistency is enforced by choosing U_{in} to be equal to U_{scf} . The second derivative with respect λ_T^I of Cococcioni type model for electron interactions in Eq(2) also corresponds to the U_{out} obtained from linear response proposed by Cococcioni et al[4]:

$$U_{out} = \frac{d^2 E_{\text{quad}}}{d(\lambda_T^I)^2} = U_{\text{scf}} - \frac{U_{in}}{m} \quad (3)$$

$$\text{where } m = 1 / \sum_i (a_i^I)^2 \quad (4)$$

Introduce the linear response method of Cococcioni et al[4]. The above Eq(4) is linear order form of effective degeneracy. To our model, we don't limit the m and U_{in} in linear relationship. And we set a non-linear form and define the m in the last conclusion of the formulation. A perquisite of this linear response method is adopting a Lagrange multiplier acting on the localized orbitals by projection operation:

$$v_{ext}^p = v_{ext} + \alpha^I \sum_m |\phi_m^I\rangle \langle \phi_m^I| \quad (5)$$

The “ p ” means “perturbed”. In this Equation, the α_I represents the amplitude of the perturbation. The α_I -dependent ground state charge density and total energy was yielded:

$$\begin{aligned} E(\alpha^I) = & \sum_{i,\sigma} \varepsilon_i^\sigma(\alpha^I) - \frac{1}{2} \int v_H [\rho_{\alpha^I}(\vec{r})] \rho_{\alpha^I}(\vec{r}) d\vec{r} \\ & + E_{xc} [\rho_{\alpha^I}] - \int v_{xc} [\rho_{\alpha^I}(\vec{r})] \rho_{\alpha^I}(\vec{r}) d\vec{r} \end{aligned} \quad (6)$$

Then, through a Legendre transformation, the total energy can be described as an electron's Hubbard orbital on-site occupation-dependent (on localized Hubbard orbitals), as follows:

$$E[\{q_I\}] = \min_{n(r), \alpha_I} \left\{ E[n(r)] + \sum_I \alpha_I (n_I - q_I) \right\} \quad (7)$$

$$E^{KS}[\{q_I\}] = \min_{n(r), \alpha_I} \left\{ E^{KS}[n(r)] + \sum_I \alpha_I^{KS} (n_I - q_I^{KS}) \right\} \quad (8)$$

$$\text{Consider the Eq(7) and (8), } E \sim \frac{U}{2} (n^2 - 1) \quad (9)$$

$$\text{And we got the } U = \frac{\partial^2 E}{\partial q^2} - \frac{\partial^2 E_{KS}}{\partial q^2} = - \left(\frac{\partial \alpha}{\partial q} - \frac{\partial \alpha_{KS}}{\partial q_{KS}} \right) \quad (10)$$

We address our point here, with applying two different Lagrange potential shifts like:

$$v_{ext}^p(a) = v_{ext} + (\alpha_a) \sum_m |\phi_m^I\rangle \langle \phi_m^I| \quad (11)$$

$$v_{ext}^p(b) = v_{ext} + (\alpha_b) \sum_m |\phi_m^I\rangle \langle \phi_m^I| \quad (12)$$

The $\sum_m |\phi_m^I\rangle \langle \phi_m^I|$ above represent the on-site occupancy of electrons from the targeted Hubbard orbitals. With Legendre transformation, we have two different forms of total energy functional equations:

$$\begin{aligned} E[\{q_I\}, (\alpha_a)] &= \min_{n(r), \alpha_I} \left\{ E[n(r)] + \sum_I (\alpha_a) (n_I - q_I) \right\} \\ &= E_{LDA/GGA} + \frac{U_{scf}}{2} \sum_I \left[\sum_i \lambda_i^I \left(\sum_j \lambda_j^I - 1 \right) \right] + \frac{U_{in}}{2} \sum_I \sum_i \lambda_i^I (1 - \lambda_i^I) \end{aligned} \quad (13)$$

$$\begin{aligned} E[\{q_I\}, (\alpha_b)] &= \min_{n(r), \alpha_I} \left\{ E[n(r)] + \sum_I (\alpha_b) (n_I - q_I) \right\} \\ &= E_{LDA/GGA} + \frac{U_{scf}}{2} \sum_I \left[\sum_i \lambda_i^I \left(\sum_j \lambda_j^I - 1 \right) \right] + \frac{U_{in}}{2} \sum_I \sum_i \lambda_i^I (1 - \lambda_i^I) \end{aligned} \quad (14)$$

In the Eq(14), we choose contribution of U_{in} in on-site Hubbard orbital as 0, but set the occupancy of on-site Hubbard orbital was shifted by energy of U_{in} in the form of Lagrange multiplier.

$$\text{set } \begin{cases} \alpha_a = a \cdot \alpha_I = \frac{\alpha_I}{U_{in}} \cdot a_0 \\ \alpha_b = U_{in} + \alpha_I \end{cases} \quad (15)$$

From the above, we give an unit potential as $a_0 = 1eV$. Then we have two different Lagrange multipliers. Meanwhile, they have the relationship like:

$$\alpha_a \cdot \alpha_b = a_0 \cdot \alpha_I + \frac{\alpha_I^2}{U_{in}} \cong a_0 \cdot \alpha_I \quad (16)$$

The reason we set the two perturbations like Eq(16) is we cannot certain about the realistic non-linear relationship between U_{in} and occupancies of orbitals. Therefore, we further simplified the method above that by removing the contribution of the second term of E_{quad} and only consider the linear response calculation at the “original point” but shifting from zero to U_{in} this time. Then solving the linear response equation of eigen value of energy functionals leads us to have the simplified Lagrange multiplier potential shifts as follows:

$$\begin{cases} E[\{q_I(a)\}, \alpha_a] = \min_{n(r), \alpha_a} \left\{ E[n(r)] + \sum_I \alpha_a [n_I - q_I(\alpha_a)] \right\} \\ E^{KS}[\{q_I(a)\}, \alpha_a] = \min_{n(r), \alpha_a} \left\{ E^{KS}[n(r)] + \sum_I \alpha_a^{KS} [n_I - q_I^{KS}(\alpha_a)] \right\} \end{cases} \quad (17)$$

$$\begin{cases} E[\{q_I(a)\}, \alpha_b] = \min_{n(r), \alpha_b} \left\{ E[n(r)] + \sum_I \alpha_b [n_I - q_I(\alpha_b)] \right\} \\ E^{KS}[\{q_I(a)\}, \alpha_b] = \min_{n(r), \alpha_b} \left\{ E^{KS}[n(r)] + \sum_I \alpha_b^{KS} [n_I - q_I^{KS}(\alpha_b)] \right\} \end{cases} \quad (18)$$

Actually, a (small) and b (large) are Lagrange multipliers from theoretical aspects. Based on the above, we can rebuild the formulation of Cococcioni’s linear response:

$$U_{out1} = - \left(\frac{\partial \alpha_I}{\partial q(a)} - \frac{\partial \alpha_I^{KS}}{\partial q(a)_{KS}} \right) = - \left(\frac{\partial \alpha_a}{\partial q(a)} - \frac{\partial \alpha_a^{KS}}{\partial q(a)_{KS}} \right) \cdot \left(\frac{U_{in}}{a_0} \right) \quad (19)$$

$$= \left(\frac{U_{in}}{a_0} \right) \left(U_{scf1}(U_{in}) - \frac{U_{in}}{m} \right)$$

$$U_{out2} = - \left(\frac{\partial \alpha_I}{\partial q(b)} - \frac{\partial \alpha_I^{KS}}{\partial q(b)_{KS}} \right) = - \left(\frac{\partial \alpha_b}{\partial q(a)} - \frac{\partial \alpha_b^{KS}}{\partial q(a)_{KS}} \right) \quad (20)$$

$$= U_{scf2}(U_{in}) = \left(\frac{a_0}{U_{in}} \right) \cdot U_{scf1}(U_{in}) = \left(\frac{a_0}{U_{in}} \right) \cdot U_{scf}(U_{in})$$

We know, the perturbation of Lagrange multiplier whatever in diagonal charge occupation matrix element or electronic potential of on-site Hubbard orbital, is equivalent to the perturbed charge induced polarization by the on-site Hubbard orbital. Consider the filled shell Hubbard orbital was strongly polarized leading the perturbation being over polarized as the full-filled orbital has strong bounded wavefunction and full-filled occupations. This taught us either U_{out1} or U_{out2} singly cannot predict the U_{scf} by U_{in} , which means the value of U_{scf} cannot be **locked** by U_{in} through the single calculation of either U_{out1} or U_{out2} . With only by consider that U_{out1} and U_{out2} have no difference, then the polarizations induced by U_{out1} and U_{out2} have been compensated. Therefore, we can reliably calculate out the U_{scf} by U_{in} .

As we recall Eq (1) and (3) to figure out the condition:

$$|U_{out2} - U_{out1}|_{U_{in}} = \left| U_{scf} \left(\frac{a_0}{U_{in}} - \frac{U_{in}}{a_0} \right) + \left(\frac{U_{in}}{a_0} \right) \left(\frac{U_{in}}{m} \right) \right|_{U_{in}} \geq 0 \quad (21)$$

The U_{out1} and U_{out2} turn to be equivalent if the Eq(21) achieve the minimum, zero. Then we have,

$$U_{scf} \left(\frac{a_0}{U_{in}} - \frac{U_{in}}{a_0} \right) + \left(\frac{U_{in}}{a_0} \right) \left(\frac{U_{in}}{m} \right) = 0 \quad (22)$$

So, we got the U_{scf} with the relationship to U_{in} at the crossover point of diagrams between $U_{out1}(U_{in})$ and $U_{out2}(U_{in})$.

$$U_{scf} = \frac{\left(\frac{U_{in}}{m} \right)}{\left(1 - \left(\frac{a_0}{U_{in}} \right)^2 \right)} \quad (23)$$

If the Eq(21) does not reach the zero, like partially-filled shell, there could be a rigid difference between two different types of perturbation:

$$|U_{out2} - U_{out1}|_{U_{in}} = \left| U_{scf} \left(\frac{a_0}{U_{in}} - \frac{U_{in}}{a_0} \right) + \left(\frac{U_{in}}{a_0} \right) \left(\frac{U_{in}}{m} \right) \right|_{U_{in}} = \Delta > 0 \quad (24)$$

Then, we need to have the first variation of the equation Eq(24)=0 and its second variation is positive, as follows:

$$\delta(U_{out2} - U_{out1})_{U_{in}} = \delta \left[U_{scf} \left(\frac{a_0}{U_{in}} - \frac{U_{in}}{a_0} \right) + \left(\frac{U_{in}}{a_0} \right) \left(\frac{U_{in}}{m} \right) \right]_{U_{in}} = 0 \quad (25)$$

So, we further get,

$$\begin{aligned} \frac{\partial}{\partial U_{in}} \left[U_{scf} \left(\frac{a_0}{U_{in}} - \frac{U_{in}}{a_0} \right) + \left(\frac{U_{in}}{a_0} \right) \left(\frac{U_{in}}{m} \right) \right]_{U_{in}} &= 0 \\ \frac{\partial^2}{\partial U_{in}^2} \left[U_{scf} \left(\frac{a_0}{U_{in}} - \frac{U_{in}}{a_0} \right) + \left(\frac{U_{in}}{a_0} \right) \left(\frac{U_{in}}{m} \right) \right]_{U_{in}} &> 0 \end{aligned} \quad (26)$$

If we choose the constant of above Eq(26) as 0 for non-fully-filled shell, then we have simplified representation of U_{scf} as follows:

$$U_{scf} = \frac{\left(\frac{2U_{in}}{m} \right)}{\left(1 + \left(\frac{a_0}{U_{in}} \right)^2 \right)} + \Delta \quad (27)$$

Then, with consider two different effective degeneracies (m_1 and m_2) for full-filled shell and partially-filled shell, we summarize two different case above that for self-consistent determine and lock the input U_{in} for determining the U_{scf} in DFT+U calculations:

$$U_{scf} = \begin{cases} \frac{\left(\frac{U_{in}}{m_1}\right)}{\left(1 - \left(\frac{a_0}{U_{in}}\right)^2\right)} & (occ = 1, \text{crossover}) \\ \left(m_1 = \frac{1}{l}\right) \\ \frac{\left(\frac{2U_{in}}{m_2}\right)}{\left(1 + \left(\frac{a_0}{U_{in}}\right)^2\right)} + \Delta & (non-crossover) \\ \left(m_2 = \left[(2l+1) - \frac{occ}{2}\right]\right) \end{cases} \quad (28)$$

Let's discuss the effective degeneracy, m , in different cases. In the case of crossover, the angular momentum is degenerated, while for non-crossover, the case turns more complicated. Then we simply give m_1 and m_2 in simple form like above. The occ is the self-consistent determined electron occupancy on the localized orbital at the zero point of energy before the perturbation. From the above Eq(28), the effective degeneracy is changed for two different cases, one is crossover and another is non-crossover. Then we split the physical or chemical problems of full-filled and partially-filled orbitals into crossover and non-crossover scenarios. They are no necessary to corresponding to each other which gives our more convenience for linear-responsed perturbation calculations. For crossover, it can either full-filled like $3d^{10}$ for Zn, Ga etc. or partially-filled like $2p^4$ for O or even $2p^3$ for N, respectively. We have already given the behavior of the U_{scf} related to the U_{in} within full-filled or non-full-filled shells with different maximum angular momentums, as shown in Figure 1 (a) and (b).

This is very possible that some elements with small radius like O and N, their electrons from localized orbitals will have more evident overlapping towards similar effects of ones in closed shell. Moreover, for non-crossover cases, the effective degeneracy is attributed to the non-fully-occupied components of localized orbitals. They have angular momentum degeneration with magnitude of $(2l+1)$. This method is not just only valid for AB binary compounds with 1:1 stoichiometric ratio. If we extend to the AB_x with different localized orbitals, then for B elements, the U_{scf} for B element will be $\frac{1}{x}U_{scf}$ for normalization. We then call our method as self-consistent **U-lock**.

It is advantageous for us to have a better understand on the cRPA and GW method in simpler ways. We see that from Eq(28), the U_{scf} has the similar representation as the constrained random phase approximation (cRPA),

$$W = \frac{v}{1 - P_r v} = \frac{U}{1 - P_f U} \quad (29)$$

as used by Nillson et al and Vaugier et al for transition metal or lanthanide oxides calculations[5, 6]. The $P = P_r + P_f$ denotes the polarization of the localized states. W is the screend Coulomb interaction and U is the Hubbard U external parameter. All we need to do in GW or cRPA calculations are to obtain the value W for characterizing the quasi-particle self-energy. This W is

similar to our U_{scf} calculations to some extent. Therefore, our self-consistent U-lock has important physical meaning that to eliminate the effect of the polarization of the electron orbital perturbation in linear response calculations in DFT + Hubbard U scheme. And our self-consistent value of U_{scf} is the equilibrium value of two different perturbations, one is the electron charge occupancy of the localized orbitals, another is the electronic potential of the localized orbitals. We illustrated our models in Figure 1 (c).

Lany and Zunger have dealt with the problem of oxygen localized hole states[15-17] in wide band gap semiconductor oxides, and proposed a their method by using a determination, which is based on a resembled Koopmans theorem[18-20]. We follow their view and look back to the basic determination of the relationship between system electron energy and its integer occupation number. As Figure 1 (d) shows, the key for the correct description of localized states is depends on the d^2E/dn^2 [21, 22]. This second derivative of E is concave feature for HF theory regarding the continuous occupation number, which is $d^2E/dn^2 < 0$, while it is a convex feature for LDA/GGA, $d^2E/dn^2 > 0$. However, the correct behavior is actually linear[21-23], which means the $d^2E/dn^2 = 0$. Therefore, our proposed method can be described as:

$$|U_{out2} - U_{out1}|_{U_{in}} = \frac{d^2E}{dn^2} = 0 \quad (30)$$

The E in Eq(30) is not the system total energy. It is actually the electronic energy with integer occupation number.

3. Calculation setup

We actualize this method into codes implemented in any plane wave DFT package like CASTEP [24], which is a form of port code have flexible combinations with LDA, GGA, and as well as screened Hartree-Fock exchange (sX) functionals on demand. Our tool will be more efficient if the structure can be treated as periodic unit cell for plane wave basis. We choose non-linear core corrected norm-conserving pseudopotentials for both cation and anion elements. As we know the norm-conserving pseudopotentials can reflect all-electron behavior for outer shell valence electrons with $|\mathbf{S-matrix}|=1$ compared to ultrasoft pseudopotentials[25, 26], so the non-linear core corrected norm-conserving pseudopotential can have better response to DFT+U calculations, especially in defects calculations[8]. Note that, our method actually obtains the almost the same U-parameter with both norm-conserving and ultrasoft pseudopotentials. This means the value we got has intrinsic physical meaning for the materials. We just use non-linear core corrected norm-conserving pseudopotential for good estimated defect states in the band gap. Moreover, this method can be utilized into amorphous solid materials like amorphous metal oxides for catalytic researches. All of our examination calculations are carried out with GGA+U scheme. The Figure 2 (a) and (b) show as the examples of our theoretical method for the systems with localized orbitals.

We further select two cases for examine the method: (1) an estimation of intrinsic defect behavior of a monolayer metal oxide like ZnO and (2) an review study of the intrinsic p-type conduction of Cu_2O , since the other bulk metal oxides or solids have been already well studied by more advanced screened-exchange, HSE or GW methods (sX)[7, 27-34]. The most difficult step is to obtain accurate electronic structures, in particular to Cu_2O as early as in 1980s by

pseudopotential-based tight-binding view[35]. The localized orbitals here we focus are range from 2p orbitals for anion elements, and 3d orbitals for cat-ion elements, respectively.

4. Results and Discussion

4.1 Bulk and Monolayer ZnO

ZnO is a wide band gap semiconductor oxide with direct gap of about 3.4 eV (in 300K), and its monolayer can be used as charge trapping layer in CMOS memory cell. Many DFT calculations have given improved electronic structures as well as the defect states by hybrid functionals and GW methods. This has also been seen in DFT+U work by Janotti et al[36]. Lany and Zunger have found that the localized hole states induced by N-doped ZnO largely affect the Fermi level (E_F) deep in the bulk ZnO[18, 37].

This leaves us a question that does the localized holes states still exist in low dimensional structure of ZnO? The neutral Zn vacancy (V_{Zn}) of ZnO will induce two localized holes in the lattice and the behavior in the low-dimension is still unclear. This may give us answer that whether monolayer of ZnO could be a good substrate for interfacing with graphene layer or similar materials.

To obtain reliable results on monolayer ZnO, we have carried out bulk properties calculations for wurtzite ZnO. The self-consistent determined U parameters have been given in Table 1, and the angular-degenerated U_{scf} for Zn-3d and O-2p can be seen in Figure 2 (a). The lattice parameters we got are 3.248 Å and 5.216 Å for a and c in hexagonal lattice, respectively. The maximum error of these is less than 2% showing a reliability of our method for bulk properties. The calculated band gap is 3.441 eV remarkably close to the experimental value near the 0K[38, 39]. The 3d level is calculated and show about 7.5 eV lower than the VBM, giving another consistency to the experimental value[38, 39]. The related bulk properties have been compared with other groups in benchmark shown in Table 2. The band structure and density of states of bulk ZnO have been presented in Figure 3 (a).

Recent study shows that the monolayer ZnO can be interfaced with graphene acting as a good substrate for topological insulator (TI), since the dirac-cone retains and is pinned near the midgap of the monolayer ZnO, regardless the existence of the intrinsic defects[40]. As shown in Figure 3 (b), we found the band structure and density of states occur tail states due to the long range crystal field interaction missing vertically to ZnO(0001), and the 3d levels have been split into two peaks due to a evident contrast of p-d coupling along and perpendicular to ZnO(0001). The band gap has widen to 3.57 eV compared to 3.441 eV in bulk phase from our calculations. The starting point of 3d level is nearly the same as in the bulk (-7.5 eV we got in calculation.). The formation entropy of the bulk ZnO is -3.70 eV which is consistent to the experimentally reported -3.60 eV in 300K. Figure 3 (a) and Figure 3 (b) give the basic electronic properties of bulk wurtzite and monolayer of ZnO, respectively.

The oxygen hole states levels have been long interested in the metal oxides or wide band gap semiconductors, particularly in the ZnO[18, 19], the localized hole levels move the Fermi level towards deep in the gap. We investigate the single zinc vacancy (V_{Zn}) as it can induce two holes localized around nearby O-sites. However, this cannot clearly given by LDA/GGA calculations

as the homogenous electron gas treats the two hole states degenerated into one and delocalized around the V_{Zn} site. Our GGA+U calculation with stabilizing the hole states can give clear electron-hole interaction under different charge states, as shown in Figure 3 (c). This has been also reported by our previous work[8]. Figure shows the neutral V_{Zn} has negative effective correlation U (negative- U_{eff}) of -0.57 eV (shown in Figure 3 (d)), for the process of $2(V_{Zn}^0) \rightarrow (V_{Zn}^+) + (V_{Zn}^-)$. Such exothermal reaction means one of the O-site acting as acceptors capturing two electrons easily overcoming the onsite Coulomb repulsive energy, which are the nearest neighbor of V_{Zn}^0 . The other two localized hole states turns to be repulsive to each other while the electron acceptor sites that move towards to the hole sites. This shows a planar Jahn-Teller distortion effect that the symmetry lowers from D_{3h} down to the D_{2h} . The other two charge states, V_{Zn}^+ and V_{Zn}^- , also have the same trends. The total energy of the system lowers with structural relaxation. From Figure 3 (e), we also found that the localized hole states have the π -like orbital next to the conduction band minimum, and perpendicular to the plane (0001) in real space with p_z -orbital character (with a_1 -symmetry). However, the electron acceptor site has similar π -like orbital along the (0001) plane, which is a feature of p_{xy} -orbital. This interesting behavior leads the monolayer ZnO system has an anti-ferromagnetic feature with existence of single neutral V_{Zn} .

Compared with the bulk case, the V_{Zn} actually have -2, -1, and 0 three charge states in the bulk ZnO and with positive correlation energy. This can be seen in the work of Clark et al[7, 28]. This means the electron-electron repulsion at the same lattice site cannot be compensated by the lattice distortions in the bulk. This address the difference between bulk and monolayer ZnO.

We can also find that the hole and electron levels are not free-charge-carrier supplying center as they are localized as trap states. The intrinsic conductivity of the monolayer ZnO may largely restricted by such native defects. The E_F was actually pinned near the midgap. If we extend the system to interface with graphene layer, the position of dirac-cone (cone level) will be pinned near the midgap of the ZnO owing to the subtle electron-holes interactions (illustrated in Figure 3 (f)). The reason that the Jahn-Teller distortion occurs in the monolayer ZnO with V_{Zn} is because the asymmetry between the occupancies of $p_{x,y}$ and p_z orbitals within the planar monolayer ZnO is getting larger than the non-centrosymmetrical bulk wurtzite ZnO. This asymmetry can be also found in ZnO but negligible[19].

3.2 Intrinsic p-type Cu_2O

We gave the variation behaviors of d and p orbitals of d^{10} -based compounds in terms of U_{out1} and U_{out2} , shown in Figure 2 (b). We see that the p orbitals of linear response have also crossover behavior similar to the d^{10} orbitals. This means the d^{10} compounds have strong p-d coupling that the p orbitals of valence electrons of anion elements tend to be full-filled for bonding with adjacent elements with d orbitals.

The origin of intrinsic p-type conductivity in Cu_2O has been an issue for a long term and this requires an intensive computation effort to interpret. Scanlon et al proposed it attributes to the Cu binding to Cu vacancy with tetrahedral coordinate (V_{Cu} -split) by HSE study, and contributes a deep localized state[32, 33]. However, Isseroff et al [34] use the same HSE method found the V_{Cu} -split has about 0.5 eV higher than normal V_{Cu} . This may due to not well counteracted oxygen hole levels. The total energy of CuO with corrected Hubbard U is also a challenging task since it provides the lower limit of Cu chemical potential for defect formation energy calculations in

Cu_2O . According to the Figure 2 (b), we got the d-orbital Hubbard correction of 6.8 eV for Cu and normalized 12 eV for O 2p orbitals. Note that the large Hubbard correction for 2p orbitals of O arise because each O site experience two Cu localized electron perturbation in linear response calculations. Meanwhile, as we found from Figure, the Cu actually presents the full-filled shell feature in Cu_2O system as it touches the 0 eV level in Figure 2 (b). But each perturbation of d-electrons has been dividedly share with one O site. Therefore, this is different to other ordinary coordinated metal oxides, as the metal atoms normally have larger coordination number to the O. The Cu_2O is a kind of reversed CaF_2 structure as O occupies the Ca site while the Cu occupies the F site. The band structures of Cu_2O and CuO in AFM phase have been shown in Figure 4 (a) and (b).

Experimentally found the acceptor-like trap states are actually two states with 0.25 and 0.45 eV higher than the VBM[41]. But with oxygen flux increased in that experiments, one of the density of the trap states increase while the other steps down to a lower density. This gives a hint that the O-related intrinsic defects may play a significant role of giving an acceptor-like trap levels near the VBM. But this requires the accurate description on the localized holes states induced by O-2p orbitals as stated previously[8]. Moreover, whether the Hubbard U parameter can improve both the electronic structure and localized hole states in the gap are anticipated.

As shown in Table 3, we find that our method can gives consistent lattice parameters together with the electronic band gap of the Cu_2O , which is 2.17 eV in experiments. Isseroff et al argue whether the $\text{V}_{\text{Cu}}^{\text{split}}$ has lower formation energy than the simple Cu vacancy. Our data shows the consistency with the Scanlon et al that the neutral $\text{V}_{\text{Cu}}^{\text{split}}$ has about 0.8 eV lower than the $\text{V}_{\text{Cu}}^{\text{simple}}$. This helps us to believe the corrected O-2p orbital energies will improve the defect formation studies. One may argue that the Hubbard U parameter correction for O-2p orbitals may be too high with magnitude of 12 eV. But our formation energies of O-interstitial defects in tetrahedral and octahedral ($\text{I}_{\text{O}}^{\text{tet}}$ and $\text{I}_{\text{O}}^{\text{oct}}$) have very similar values to the data given by HSE with HF interaction percentage of 0.375 in the work of Scanlon et al. Thus, the O-2p orbital correction in terms of Hubbard U will not affect the defect formation energies as well as the thermal dynamic transition levels in different charges, the work of Cu_2O presented by us here is to show the robustness of the DFT+ U_{scf} in both localized d/f orbitals of cations and p orbitals of anions.

We show in Figure 4 (c) that the contribution of p-type intrinsic conductivity of Cu_2O is actually not coming from V_{Cu} -split. The formation energies of V_{Cu} -split and simple V_{Cu} have the similar trend to the work of Scanlon et al. and the V_{Cu} -split has about 0.6 eV lower than the simple V_{Cu} . This confirms the Cu atom favors flexible structural relaxation to a more stably tetrahedral coordination. However, this is not the lowest energy defect, neither the oxygen vacancy (V_{O}). It is actually the oxygen interstitials (I_{O}). Experiments show that the Cu_2O stabilized in high-temperature condition since it has the reaction process from CuO like: $4\text{CuO} \rightarrow 2\text{Cu}_2\text{O} + \text{O}_2\uparrow$. We see that the Cu_2O structure has many hollow channels for oxygen diffusion through. The excess O actually may be trapped in this channel induced localized states to capture electrons. We found the tetrahedral I_{O} (I_{Otet}) has even lower formation energy than the V_{Cu} -split.

In electronic properties (shown in Figure 4 (d)), the V_{Cu} -split give an very deep localized hole states next to the conduction band minimum (CBM), which has a d-orbital feature. The simple V_{Cu} has a localized state with 0.4 eV higher than the valence band maximum (VBM). We see

that the I_{Otet} has two localized states with 0.2 eV and 0.5 eV higher than the VBM. This is close to the observations of experiments, whose trap states are reported to be 0.25 eV and 0.45 eV higher than the VBM[41]. The formation energy of I_{Otet} has about 0.3 eV lower than the V_{Cu} -split. This results are found only based on the well counteracted the self-interaction induced by localized hole states. Therefore, we argue that the experimentally reported intrinsic p-type conduction was actually contributed by both V_{Cu} ^{split} and O-interstitial intrinsic defects in the Cu_2O . They have almost close formation energy within the range between (0/-1) and (-1/-2) transition states, with two single-particle trapping levels higher than VBM.

5. Conclusion

We have shown that using our proposed two-way linear response method can find out the on-site screened Coulomb potential for the full-filled shell metal oxides for both cations and anions. This method can also tell the orbital shell is whether has the tendency of being full-filled or not as whether it can approach to the 0 eV. By this method, we applied our self-consistently determined on-site Coulomb potential to the Hubbard U parameters of d and p orbitals for cations and anions, respectively. We got close results to the experimental data on the electronic and atomic properties of full/nearly filled shell metal oxides or solids. Moreover, we extends our study to the defects states of low-dimensional and other interesting system, we found this method can give not just quick answer on the electronic structures of the eigen-bulk properties but also the satisfied native defect levels of the bulk or low dimensional structures. This will accelerate our research and discover (R&D) pace for electronic engineering of the new generation of materials which forms or being synthesized under the extreme physical or chemical environments.

Reference

- [1] F. Aryasetiawan and O. Gunnarsson, Rep. Prog. Phys. **61**, 237 (1998).
- [2] I. A. Vladmir, F. Aryasetiawan, and A. I. Lichtenstein, J. Phys.: Condens. Matter **9**, 767 (1997).
- [3] A. Svane and O. Gunnarsson, Phys. Rev. Lett. **65**, 1148 (1990).
- [4] M. Cococcioni and S. de Gironcoli, Phys. Rev. B **71**, 035105 (2005).
- [5] L. Vaugier, H. Jiang, and S. Biermann, Phys. Rev. B **86**, 165105 (2012).
- [6] F. Nilsson, R. Sakuma, and F. Aryasetiawan, Phys. Rev. B **88**, 125123 (2013).
- [7] S. J. Clark and J. Robertson, Phys. Rev. B **82**, 085208 (2010).
- [8] B. Huang, R. Gillen, and J. Robertson, J. Phys. Chem. C **118**, 24248 (2014).
- [9] R. Pentcheva and W. E. Pickett, Phys. Rev. B **74**, 035112 (2006).
- [10] A. K. McMahan, R. M. Martin, and S. Satpathy, Phys. Rev. B **38**, 6650 (1988).
- [11] O. Volnianska, T. Zakrzewski, and P. Boguslawski, J. Chem. Phys. **141**, 114703 (2014).
- [12] L. A. Agapito, S. Curtarolo, and M. Buongiorno Nardelli, Physical Review X **5**, 011006 (2015).
- [13] P. H. Dederichs, S. Blügel, R. Zeller, and H. Akai, Phys. Rev. Lett. **53**, 2512 (1984).
- [14] H. J. Kulik, M. Cococcioni, D. A. Scherlis, and N. Marzari, Phys. Rev. Lett. **97**, 103001 (2006).
- [15] G. Pacchioni, F. Frigoli, D. Ricci, and J. A. Weil, Phys. Rev. B **63**, 054102 (2000).
- [16] M. d'Avezac, M. Calandra, and F. Mauri, Phys. Rev. B **71**, 205210 (2005).
- [17] A. Droghetti, C. D. Pemmaraju, and S. Sanvito, Phys. Rev. B **78**, 140404 (2008).
- [18] S. Lany and A. Zunger, Phys. Rev. B **80**, 085202 (2009).

- [19] S. Lany and A. Zunger, *Phys. Rev. B* **81**, 205209 (2010).
- [20] A. Zunger and A. J. Freeman, *Phys. Rev. B* **16**, 2901 (1977).
- [21] J. P. Perdew, A. Ruzsinszky, G. I. Csonka, O. A. Vydrov, G. E. Scuseria, V. N. Staroverov, and J. Tao, *Phys. Rev. A* **76**, 040501 (2007).
- [22] P. Mori-Sánchez, A. J. Cohen, and W. Yang, *Phys. Rev. Lett.* **100**, 146401 (2008).
- [23] J. P. Perdew, R. G. Parr, M. Levy, and J. L. Balduz, *Phys. Rev. Lett.* **49**, 1691 (1982).
- [24] S. J. Clark, M. D. Segall, C. J. Pickard, P. J. Hasnip, M. I. J. Probert, K. Refson, and M. C. Payne, *Z. Kristallogr.* **220**, 567 (2005).
- [25] P. J. Hasnip and C. J. Pickard, *Comput. Phys. Commun.* **174**, 24 (2006).
- [26] K. Laasonen, A. Pasquarello, R. Car, C. Lee, and D. Vanderbilt, *Phys. Rev. B* **47**, 10142 (1993).
- [27] S. J. Clark, J. Robertson, S. Lany, and A. Zunger, *Phys. Rev. B* **81**, 115311 (2010).
- [28] S. J. Clark and J. Robertson, *physica status solidi (b)* **248**, 537 (2011).
- [29] R. Gillen, S. J. Clark, and J. Robertson, *Phys. Rev. B* **87**, 125116 (2013).
- [30] S. Lany and A. Zunger, *Phys. Rev. B* **81**, 113201 (2010).
- [31] M. Heinemann, B. Eifert, and C. Heiliger, *Phys. Rev. B* **87**, 115111 (2013).
- [32] D. O. Scanlon, B. J. Morgan, G. W. Watson, and A. Walsh, *Phys. Rev. Lett.* **103**, 096405 (2009).
- [33] D. O. Scanlon and G. W. Watson, *Phys. Rev. Lett.* **106**, 186403 (2011).
- [34] L. Y. Isseroff and E. A. Carter, *Chem. Mater.* **25**, 253 (2013).
- [35] J. Robertson, *Phys. Rev. B* **28**, 3378 (1983).
- [36] A. Janotti and C. G. Van de Walle, *Phys. Rev. B* **76**, 165202 (2007).
- [37] S. Lany and A. Zunger, *Phys. Rev. B* **81**, 205209 (2010).
- [38] D. C. Reynolds, D. C. Look, B. Jogai, C. W. Litton, G. Cantwell, and W. C. Harsch, *Phys. Rev. B* **60**, 2340 (1999).
- [39] W. Göpel, J. Pollmann, I. Ivanov, and B. Reihl, *Phys. Rev. B* **26**, 3144 (1982).
- [40] Q. Yao, Y. Liu, R. Lu, C. Xiao, K. Deng, and E. Kan, *Rsc Advances* **4**, 17478 (2014).
- [41] G. K. Paul, Y. Nawa, H. Sato, T. Sakurai, and K. Akimoto, *Appl. Phys. Lett.* **88**, 141901 (2006).
- [42] R. T. Girard, O. Tjernberg, G. Chiaia, S. Söderholm, U. O. Karlsson, C. Wigren, H. Nylén, and I. Lindau, *Surf. Sci.* **373**, 409 (1997).
- [43] K. Ozawa, K. Sawada, Y. Shirotori, and K. Edamoto, *J. Phys.: Condens. Matter* **17**, 1271 (2005).
- [44] G. Seguini, E. Bonera, S. Spiga, G. Scarel, and M. Fanciulli, *Appl. Phys. Lett.* **85**, 5316 (2004).
- [45] J. S. Blakemore, *J. Appl. Phys.* **53**, R123 (1982).
- [46] J. Ma, B. Garni, N. Perkins, W. L. O'Brien, T. F. Kuech, and M. G. Lagally, *Appl. Phys. Lett.* **69**, 3351 (1996).
- [47] H. M. Upadhyaya and S. Chandra, *J. Mater. Sci.* **29**, 2734 (1994).
- [48] D. Vogel, P. Krüger, and J. Pollmann, *Phys. Rev. B* **55**, 12836 (1997).
- [49] F. Oba, A. Togo, I. Tanaka, J. Paier, and G. Kresse, *Phys. Rev. B* **77**, 245202 (2008).
- [50] H. Raebiger, S. Lany, and A. Zunger, *Phys. Rev. B* **76**, 045209 (2007).
- [51] A. Soon, X.-Y. Cui, B. Delley, S.-H. Wei, and C. Stampfl, *Phys. Rev. B* **79**, 035205 (2009).
- [52] M. Nolan and S. D. Elliott, *Phys. Chem. Chem. Phys.* **8**, 5350 (2006).
- [53] D. R. Lide, (CRC Press], Boca Raton, FL, 2012).

Table 1. Comparison of the calculated PBE+U(scf) on binary filled shell compounds to the experimental results. The experimental band gap are referred to the ones from 0K. (Refs. [7, 31, 42-48])

Compound	U _d (scf) (eV)	U _p (scf) (eV)	Lattice (Å)	EXP. Lattice (Å)	E _g (eV)	EXP. E _g (eV)	E _{d/f} (eV)	EXP. E _{d/f} (eV)
ZnO (hex)	11.238	6.502	3.248/5.216	3.249/5.205	3.441	3.44	-7.5	-7.3
ZnS (cub)	13.083	5.174	5.470	5.409	3.846	3.8	-10.7	
CdO (cub)	10.102	6.862	4.704	4.695	1.379/ 2.459	2.3(dir)	-7.8	
CdS (cub)	13.210	5.061	5.893	5.832	2.652	2.4	-12.3	
GaN (cub)	17.878	6.866	4.552	4.540	3.534	3.504	-21.2	-22.2
GaP (cub)	17.513	4.802	5.567	5.450	2.491	2.32	-22.6	
GaAs (cub)	16.205	4.779	5.717	5.653	1.755	1.519	-22.8	-22
Cu ₂ O	6.850	13.122	4.276	4.270	2.159	2.17	-4.5 to 0	
CuO (AFM)	6.361	4.322	4.558/3.644/ 5.207	4.653/3.410/ 5.108	1.681	1.7	-9.5 to -2	
Lu ₂ O ₃ (hex)	13.976	5.467	3.604/5.812		5.584	5.5	-6.8	
Lu ₂ O ₃ (cub)	12.307	5.497	10.472	10.391	5.528	5.5	-6.0	-5.8

Table 2. Benchmark of the present work with other calculation methods in different packages.

	Benchmark	a (Å)	c (Å)	E _g (eV)	E _{3d} (eV)	ΔH _f (eV)	Vo (O-poor)	Refs
VASP	PBE_PAW_U	3.148	5.074	1.51	-6.0	-3.50	3.72	[36]
	PAW_HSE	3.261	5.225	2.49	-5.8	-3.01	0.96	[49]
	PAW_HSE_(0.375)	3.249	5.196	3.43	-6.4	-3.13	1.01	[49]
	PAW_GW		3.34					[30]
CASTEP	PBE+NoNLCC	3.286	5.299	0.90	-4.8	-2.93		[27, 28]
	PBE+NLCC	3.278	5.301	1.04	-4.0	-3.20		[this work]
	sX	3.267	5.245	3.41	-7.0	-3.31	0.85	[27, 28]
Exp.	PBE+U(scf)+NLCC	3.248	5.216	3.441	-7.53	-3.70	0.963	[this work]
	Exp. (1)	3.242	5.188	3.44	-7.5	-3.63		[38, 39]
	Exp. (2)	3.249	5.205	3.44	-7.3			[42, 43]

Table 3. Comparison of the bulk properties, formation enthalpies of Cu₂O and CuO (AFM), defect formation energies in (Cu-rich/O-poor), single-particle levels, and transition energies between present work and results from other groups.

		PBE[50]	GGA [51]	PBE+U [52]	PBE+U [34]	HSE(0.275) [34]	HSE(0.275) [32]	This work	Exp[53]
	Lattice (Å)	4.31	4.32					4.28	4.27
	Eg	0.43	0.46	0.4		2.12	2.12	2.16	2.17
ΔH_f	Cu ₂ O		-1.24		-1.64	-1.62	-1.59	-1.79	-1.75
	CuO				-1.21	-1.44	-1.46	-1.74	-1.63
	V_{Cu}^{simple}	0.70	0.47	0.41	1.10	1.34	1.15	3.20	
$\Delta H_f(D, 0)$ (eV)	V_{Cu}^{split}	1.00	0.78	0.47	1.28	1.58	1.14	2.48	
	I_O^{oct}	1.80	1.90				1.94	2.12	
	I_O^{tet}	1.30	1.47				1.87	2.19	
	V_O	0.80	0.90				1.20	2.62	
	V_{Cu}^{simple}	0.00	0	0.00			0.52	0.11	
Single-particle level (eV)	V_{Cu}^{split}				0.57		1.12	0.16	
	I_O^{oct}						1.14	0.31	
	I_O^{tet}						1.05	0.41	
	V_O							0.44	
$(-1/0)$ (eV)	V_{Cu}^{simple}	0.28	0.18				0.23	-0.89	
	V_{Cu}^{split}	0.29	0.20				0.47	0.08	
	I_O^{oct}	0.66	0.45				1.08	0.55	
	I_O^{tet}	0.78	0.65				1.27	0.39	

Figure 1

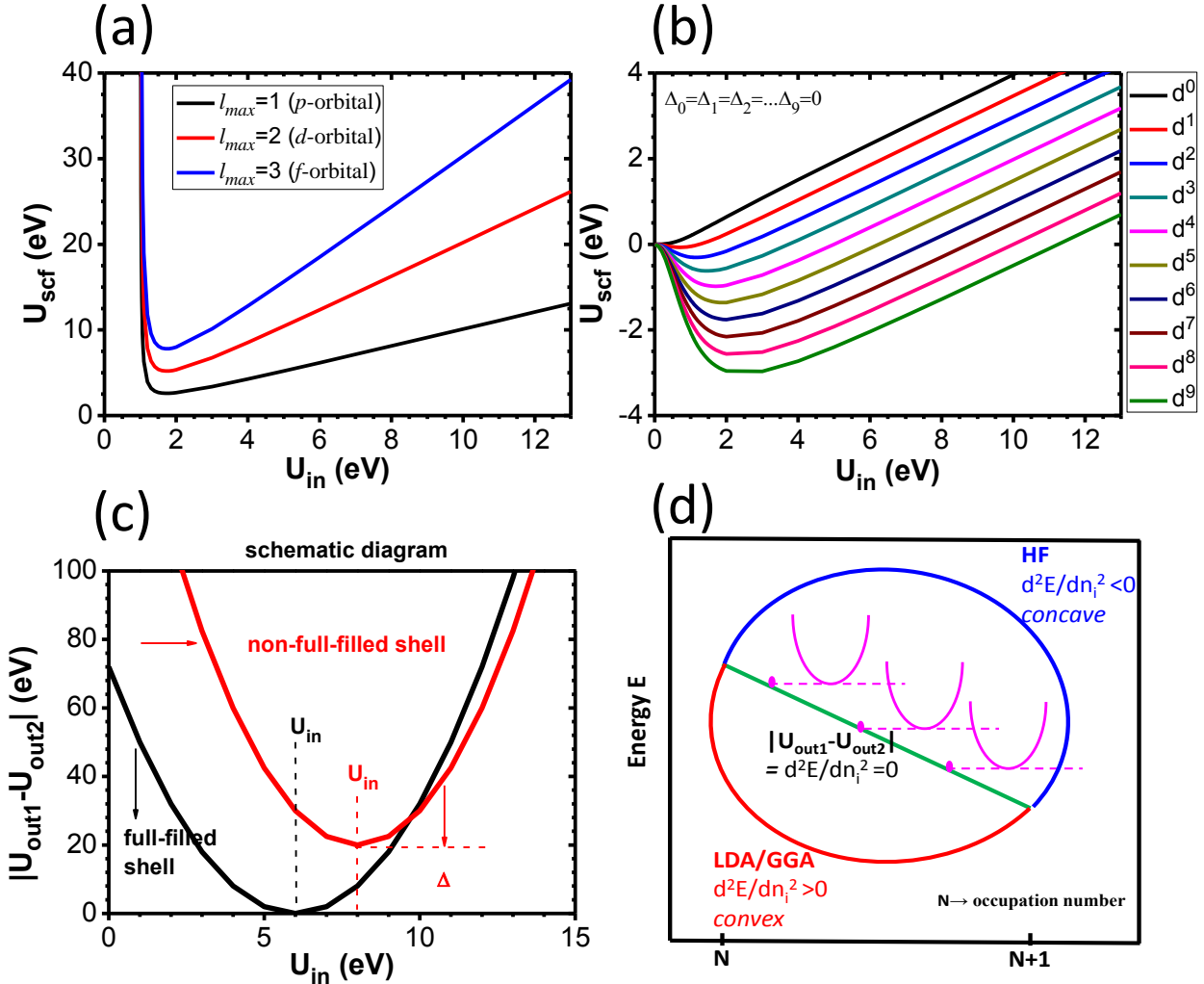


Figure 1. (a) Full-filled shell on-site screened Coulomb potential U_{scf} vs U_{in} with different maximum angular momentum. (b) Non-full-filled shell on-site screened Coulomb potential U_{scf} vs U_{in} with different d orbital occupancies. (c) The $|U_{out1}-U_{out2}|$ vs U_{in} behaviors varied by full-filled and non-full-filled shells. (d) Electronic energy vs integer/fractional occupation numbers with different theoretical models for dealing with many-body calculations.

Figure 2

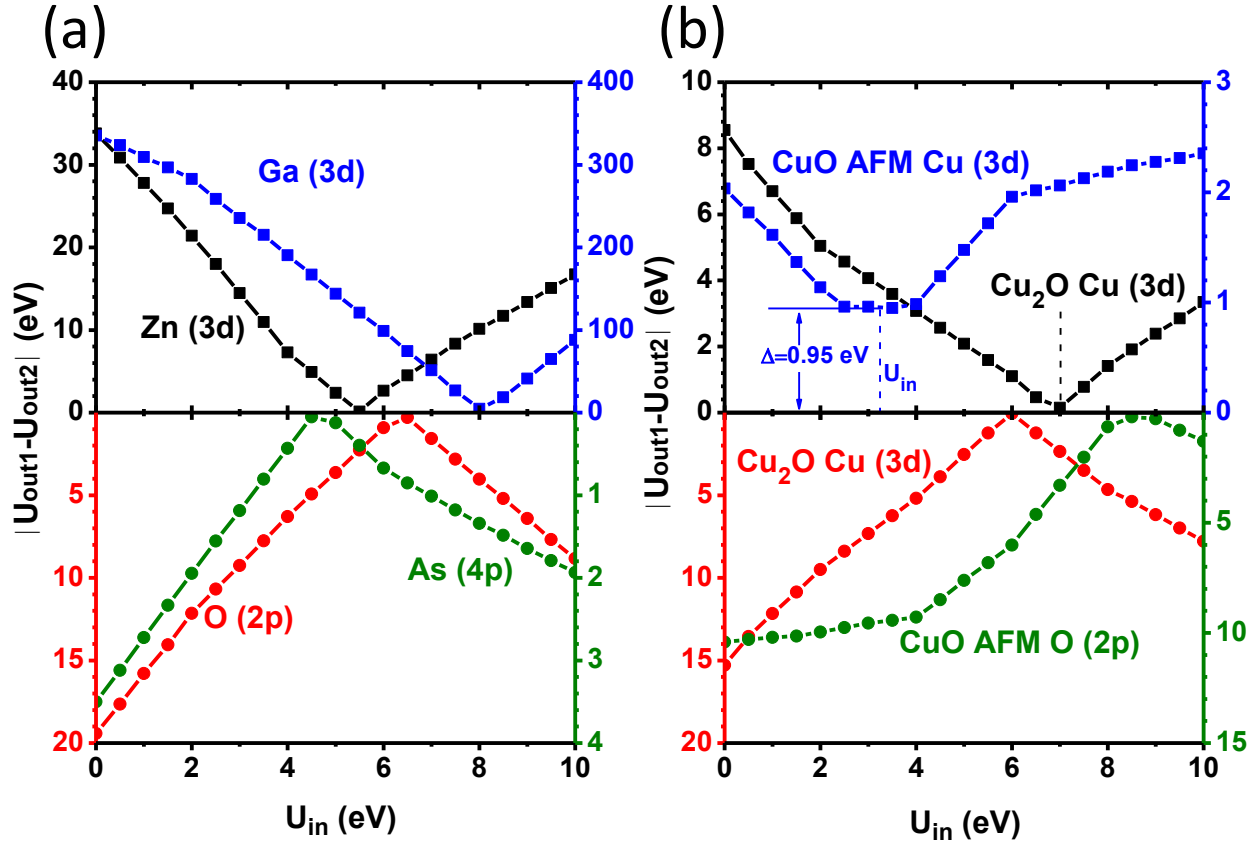


Figure 2. The $|U_{out1} - U_{out2}|$ vs U_{in} behaviors of bulk wurtzite ZnO, wurtzite GaN, bulk CuO in AFM phase, and bulk Cu₂O structures with d and p localized electronic orbitals. (AFM: anti-ferromagnetic).

Figure 3

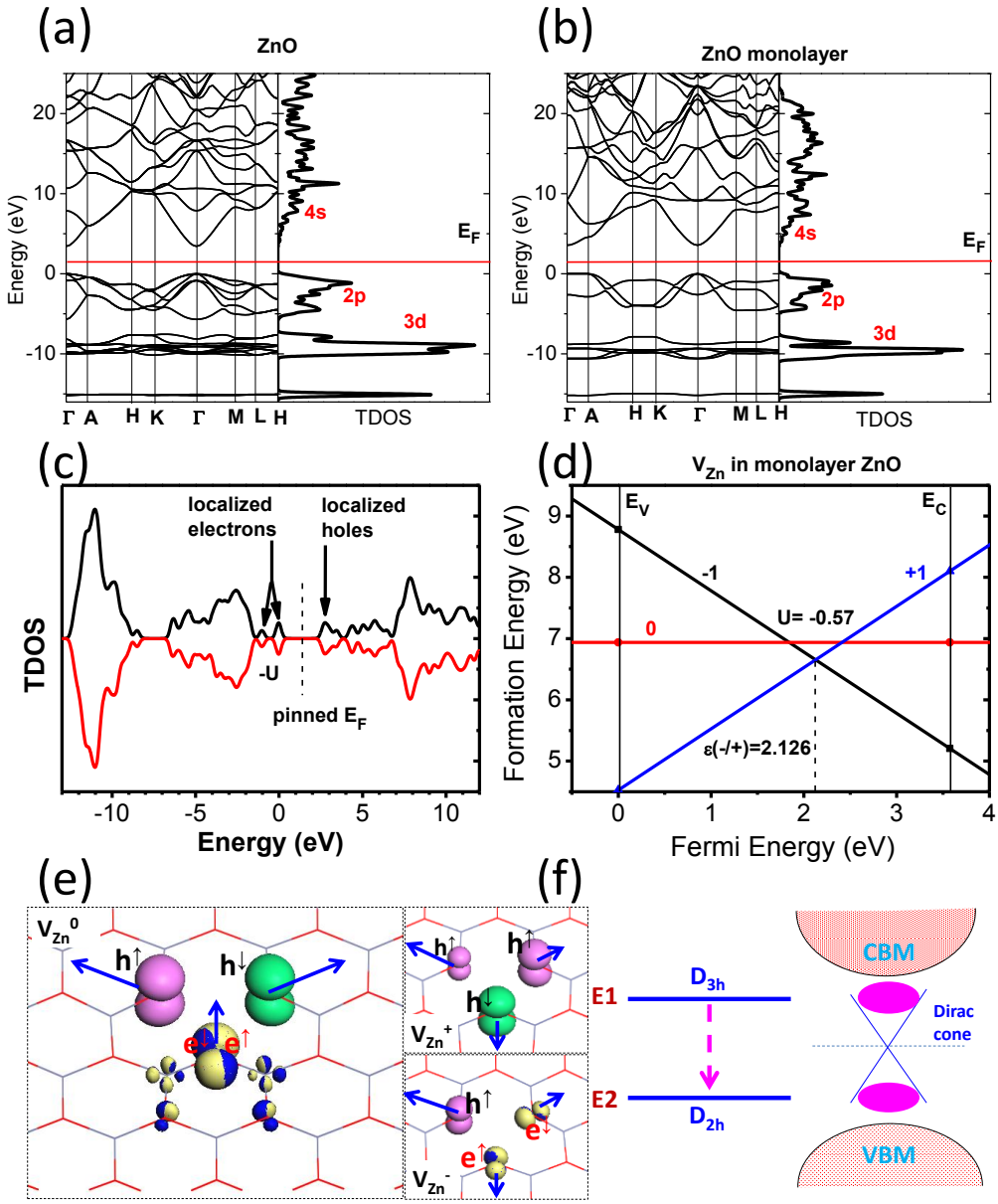


Figure 3. (a) Electronic band structure and total density of states (TDOS) of wurtzite ZnO with estimated band gap of 3.407 eV. (b) Electronic band structure and total density of states (TDOS) of planar monolayer ZnO with estimated band gap of 3.573 eV. (c) TDOS of monolayer ZnO system with intrinsic neutral Zn vacancy (V_{Zn}^0). (d) Formation energy vs Fermi energy within different charge states of -1, 0, and +1, for V_{Zn} in monolayer of ZnO. (e) Localized orbitals electron and oxygen hole states that near the edges of valence and conduction band edges within charge states of -1, 0, and +1 (Zn=grey, O=red, spin-up hole state=pink, spin-down hole state=green, and spin-up and spin-down electrons=golden and blue). (f) Schematic diagram of the energy lowering down with the symmetry lowers down from D_{3h} to D_{2h} , and the dirac-cone levels was pinned in the mid-gap of the host monolayer of ZnO within the system of grapheme/monolayer ZnO.

Figure 4

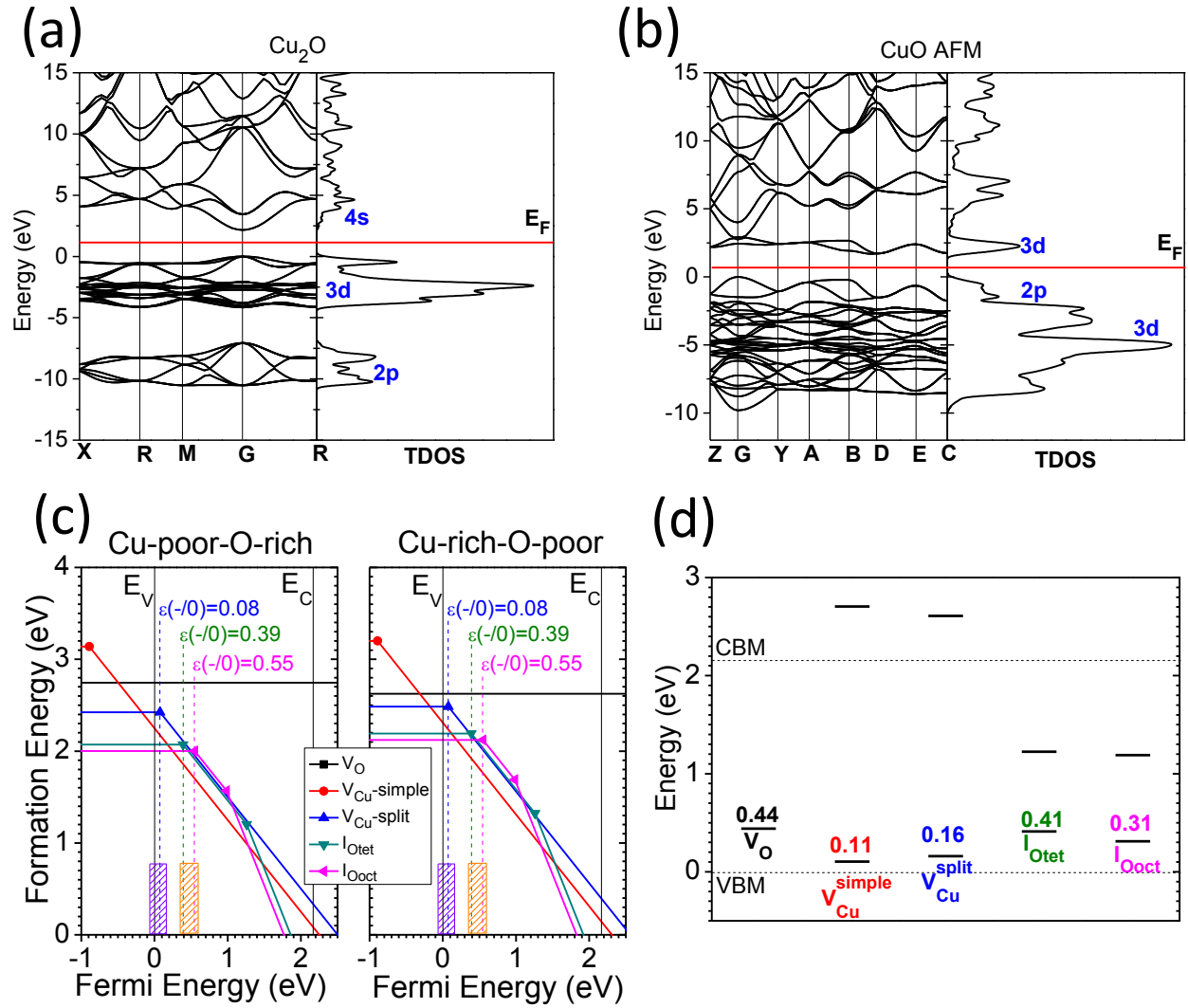


Figure 4. (a) Electronic band structure and TDOS of the bulk Cu₂O. (b) Electronic band structure and TDOS of CuO in AFM phase. (c) Formation energies summary of the intrinsic defects in Cu₂O within two different chemical potential limits. (d) The electronic localized states within the band gap of Cu₂O in related to the intrinsic defects, which reflects the intrinsic p-type conduction behavior of the Cu₂O.